



Cite this: DOI: 10.1039/c5dt00742a

Synthesis, structural studies, kinetic stability, and oxidation catalysis of the late first row transition metal complexes of 4,10-dimethyl-1,4,7,10-tetraazabicyclo[6.5.2]pentadecane†

Dallas L. Matz,^a Donald G. Jones,^a Kimberly D. Roewe,^a Michael-Joseph Gorbet,^a Zhan Zhang,^b Zhuqi Chen,^b Timothy J. Prior,^c Stephen J. Archibald,^c Guochuan Yin^{*b} and Timothy J. Hubin^{*a}

Synthetic details for 4,11-dimethyl-1,4,8,11-tetraazabicyclo[6.5.2]pentadecane, the dimethyl ethylene cross-bridged homocyclen ligand are presented for the first time. Its novel Mn²⁺, Fe²⁺, Mn³⁺, and Fe³⁺ complexes have been synthesized and characterized. X-ray crystal structures were obtained for both manganese complexes, along with five additional Co³⁺, Cu²⁺, and Zn²⁺ structures, the first structural characterization of complexes of this ligand. Each complex has the *cis*-V configuration of the cross-bridged macrocycle ring, leaving *cis* labile binding sites for interaction of the complex with oxidants and/or substrates. The copper(II) complex kinetic stability in 5 M HCl and at elevated temperatures was determined and compared to related complexes in the literature. The electronic properties of the manganese and iron complexes were evaluated using solid state magnetic moment determination and acetonitrile solution electronic spectroscopy, revealing high spin metal complexes in all cases. Cyclic voltammetry in acetonitrile of the divalent iron and manganese complexes revealed reversible redox processes, suggesting catalytic reactivity involving electron transfer processes are possible for both complexes. Screening of the Mn²⁺ and Fe²⁺ complexes for oxidation catalysis using hydrogen peroxide as the terminal oxidant showed both complexes are worthy of continued development.

Received 19th February 2015,

Accepted 1st April 2015

DOI: 10.1039/c5dt00742a

www.rsc.org/dalton

Introduction

Dimethyl ethylene cross-bridged tetraazamacrocycles introduced this important class of topologically constrained ligand multiple decades ago with cyclam-based **Me₂EBC**¹ and cyclen-based **Me₂Bcyclen**² the primordial examples (Fig. 1). As the field's founder, Weisman quickly succeeded the dimethyl versions and established a flexible debenzoylation route³ to the "parent" dihydro versions that could be substituted with a myriad of pendant arms and produced a number of highly

useful ⁶⁴Cu PET imaging agents.^{4–14} Only recently has the imaging community incorporated the 13-membered macrocycle "homocyclen" with the production of **CB-TR2A**¹⁵ and another homocyclen-based cross-bridged ligand (**L1**, Fig. 1) produced by another group¹⁶ with bioconjugation for targeted imaging applications as a stated goal.

Concurrent with the imaging applications of pendant-armed cross-bridged tetraazamacrocycles, Busch, with some of us, embraced the original dimethyl ligands **Me₂EBC** and **Me₂Bcyclen** as ideal chelates for manganese and iron for the purpose of oxidation catalysis in harsh aqueous media.^{17–30} As rigidly bridged macrocycles, these small cryptands would provide complementary binding sites for these redox active metal ions, yet resist stepwise protic removal and deactivation of the potential catalysts as their oxide forms. The methyl versions of the ligands were actually preferred as they made all of the nitrogen atoms tertiary, and thus more resistant to ligand oxidation; did not chelate the metal ion, allowing two *cis* open sites on the metal ion for oxidant and substrate binding and activation; and even provided just enough steric bulk to prevent dimerization and inactivation of the catalysts as the oxo-bridged forms.³¹

^aDepartment of Chemistry and Physics, Southwestern Oklahoma State University, Weatherford, OK 73096, USA. E-mail: tim.hubin@swosu.edu

^bKey Laboratory for Large-Format Battery Materials and Systems, Ministry of Education, School of Chemistry and Chemical Engineering, Hubei Key Laboratory of Material Chemistry and Service Failure, Huazhong University of Science and Technology, Wuhan 430074, P. R. China

^cDepartment of Chemistry, The University of Hull, Cottingham Road, Hull HU6 7RX, UK

† Electronic supplementary information (ESI) available: Discussion of the hydrogen bonding in the crystal structures of this work. CCDC 1049977–1049983. For ESI and crystallographic data in CIF or other electronic format see DOI: 10.1039/c5dt00742a

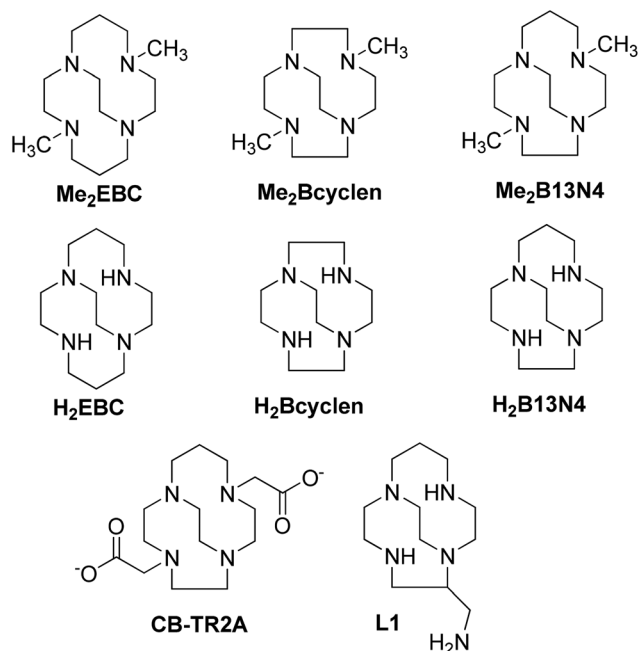


Fig. 1 Ethylene cross-bridged tetraazamacrocycles discussed in this work.

With growing understanding of the lead catalyst from this series, $\text{Mn}(\text{Me}_2\text{EBC})\text{Cl}_2$,^{32,33} we have recently begun to explore the oxidation chemistry of closely related $\text{Mn}(\text{Me}_2\text{Bcyclen})\text{Cl}_2$ ³⁴ and found interesting effects of Ca^{2+} and Cl^- on its oxidation catalysis. Having published cobalt,³⁵ nickel,³⁶ copper,³⁷ and zinc³⁷ complexes of **Me₂B13N4** (Fig. 1), we set out to synthesize the manganese and iron analogues and screen them for catalytic oxidation chemistry for comparison to the cyclam and cyclen analogues. An additional goal was to obtain X-ray crystal structures of any transition metal complexes with **Me₂B13N4** that we could, as previous attempts in our hands at structural characterization of complexes of this ligand had been unsuccessful. Below, we present synthetic details, seven X-ray crystal structures of **Me₂B13N4** complexes, and chemical characterization and oxidation screening of the biomimetically relevant $\text{Fe}(\text{Me}_2\text{B13N4})\text{Cl}_2$ and $\text{Mn}(\text{Me}_2\text{B13N4})\text{Cl}_2$ complexes.

Results and discussion

Synthesis

Dimethyl cross-bridged cyclam, **Me₂EBC**¹ was the first ethylene cross-bridged tetraazamacrocycle and was first synthesized by Weisman's route utilizing the regiospecific bis-methylation of the cyclam-glyoxal condensate bisaminal, followed by ring-opening reduction by sodium borohydride.¹ **Me₂Bcyclen** was initially synthesized by another route,² but was stated³⁸ to have been described as part of the general synthetic procedure for producing the "parent" cross-bridged ligands. In this route, alkylation of the glyoxal condensates of cyclen, homocyclen,

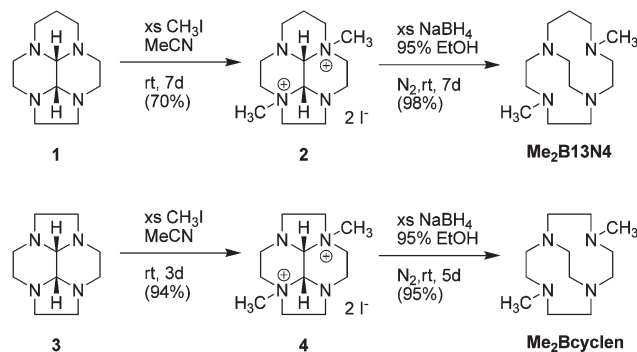


Fig. 2 Synthetic scheme for the synthesis of **Me₂B13N4** and **Me₂Bcyclen**.

and cyclam is achieved using benzyl bromide, which is followed by ring opening and debenzylation to give two secondary amines.³ However, this ref. 3 in fact does not describe **Me₂Bcyclen** or **Me₂B13N4** as part of the general scheme or at all. A later publication⁴ contains synthetic details on **Me₂EBC** only, but again not on **Me₂Bcyclen** or **Me₂B13N4**. Although we have been making references in our own publications^{35–37} to these papers^{1,3,4} for nearly two decades for the syntheses of **Me₂Bcyclen** and **Me₂B13N4**, only during the preparation of this manuscript did we discover that synthetic details specific to neither of these two ligands actually appear anywhere in the literature, other than Bencini's original synthesis of **Me₂Bcyclen** by another route.² We therefore present those synthetic details in the Experimental section. Fig. 2 shows the synthetic scheme for **Me₂B13N4** and **Me₂Bcyclen**.

The chemistry is entirely analogous to the synthesis of **Me₂EBC**,⁴ with regiospecific dimethylation in high yields in both cases the key synthetic step. The dimethyl cyclen glyoxal has been prepared under different conditions by Handel³⁹ and Lukes,⁴⁰ but is included for completeness. Sodium borohydride ring opening reduction, again under conditions suggested for **Me₂EBC**,⁴ gives the smaller cross-bridged ligands in similar yields as colorless oils after vacuum distillation from KOH.

Complexation of **Me₂B13N4** with manganese and iron were carried out to produce novel complexes that may have interesting catalytic oxidation behavior, as do their **Me₂EBC**^{17–29} and **Me₂Bcyclen**³⁴ analogues. Reaction of the ligand in acetonitrile with anhydrous MnCl_2 and FeCl_2 in an inert atmosphere glovebox gave good yields of the $\text{M}(\text{Me}_2\text{B13N4})\text{Cl}_2$ complexes. Oxidation of these divalent complexes by molecular bromine in methanol in the presence of NH_4PF_6 resulted in the immediate precipitation of $[\text{M}(\text{Me}_2\text{B13N4})\text{Cl}_2]\text{PF}_6$ trivalent complexes.

Complexation with other metal ions were typically repeated from previous work that has already been published.^{35–37} The goal of re-making cobalt, copper, and zinc complexes was to try again to obtain X-ray crystal structures to compare with the ones obtained from the manganese complexes and with the **Me₂EBC** and **Me₂Bcyclen** complexes from earlier work. Fortunately, we were successful in a number of cases, where we

had been unsuccessful in our earlier works, and we now present a total of seven X-ray crystal structures of **Me₂B13N4** below. One new zinc(II) complex was synthesized from zinc acetate in acetonitrile, followed by anion metathesis to give the [Zn(**Me₂B13N4**)(OAc)(H₂O)]PF₆ complex, which is also structurally characterized below.

Single crystal X-ray crystallographic studies

As far as we are aware, the only published crystal structure of an ethylene cross-bridged homocyclen is the copper complex of **CB-TR2A**. With its two acetate pendant arms, this hexadentate ligand coordinatively saturates the copper(II) ion.¹⁵ We report seven new structures of **Me₂B13N4** complexes here, a tetradentate ligand allowing for greater variability in coordination of the two open coordination sites and more similar to the large number of **Me₂Bcyclen** and **Me₂EBC** complexes previously published and to which we can turn to for comparison. Table 1 lists crystal data for these seven new crystal structures. Table 2 lists selected bond lengths and angles. Fig. 3–11 contain views of the X-ray crystal structures and will be referred to in the discussion that follows.

General observations about the series of **Me₂B13N4** structures

Several general observations can be made about this collection of crystal structures, before descriptions of the individual structures are made. First, the *cis*-V conformation expected to be dictated by the ligand cross-bridge is apparent for all of the complexes structurally characterized here. This result is one of the reasons to use ethylene cross-bridged tetraazamacrocycles, as the bridge forces the *cis*-V conformation, allowing two *cis* labile sites for binding oxidant and substrate next to each other, in the case of prospective oxidation catalysts.³¹

Second, the size of the metal ion influences how much distortion away from the preferred octahedral coordination geometry is required due to the short two-carbon cross-bridge, which does not allow the ligand to fully embrace larger cations. Fig. 3 illustrates the easing of this distortion, most apparent in the axial N_{ax}–M–N_{ax} bond angle that becomes more linear, for example from Fig. 3a–c. As the metal ionic radius decreases from 97 pm for 6-coordinate Mn²⁺ to 79 pm for 6-coordinate Mn³⁺ to 76 pm for 6 coordinate Co³⁺, the corresponding N_{ax}–M–N_{ax} bond angles increase from 150.29(10)° to 158.3(4)° to ~171°, respectively (two examples: 170.59(10)° and 171.2(2)°).

Finally, in comparison to the many published examples of the closely related **Me₂EBC** and **Me₂Bcyclen** transition metal complex structures, it is apparent that the ring size of the **Me₂B13N4** macrocycle makes a clear difference in how fully the metal ion is engulfed by the bridged macrocycle. Table 3 illustrates this trend, as well as giving further data illustrating the influence of the effect of the metal ionic radius within a given ligand. As expected, but not illustrated by structural data until now, the **Me₂B13N4** ligand generally produces N_{ax}–M–N_{ax} and N_{eq}–M–N_{eq} bond angles intermediate to those of the larger **Me₂EBC** and smaller **Me₂Bcyclen** ligands, given the same metal ion and coordination environment.

Table 1 Crystallographic data. L = **Me₂B13N4**^a

Chemical formula	[MnCl ₂] sja25_07 DLM10A	[MnCl ₂]PF ₆ sja17_07 DLM10B	[CoCl ₂]PF ₆ sja27_14 DGJ031	[CoCl ₂]PF ₆ CH ₃ CN sja27b_14 DGJ031	[CuCl ₂]Cl 2H ₂ O sja26_14 DGJ033	[ZnCl ₂](H ₂ O) ₂ [ZnCl ₂]-CH ₃ CN sja28_14 DGJ034	[ZnLOAcH ₂ O] PF ₆ sja23_09 KS47
C ₁₃ H ₂₈ Cl ₂ MnN ₄	C ₁₃ H ₂₈ Cl ₂ CoF ₆ N ₄ P	C ₁₃ H ₂₈ Cl ₂ CoF ₆ N ₄ P	C ₁₃ H ₂₈ Cl ₂ CoF ₆ N ₄ P	C ₁₃ H ₃₁ Cl ₂ CoF ₆ N ₄ P	C ₁₃ H ₃₂ Cl ₂ CuN ₄ O ₂	C ₂₈ H ₆₃ Cl ₆ N ₉ O ₂ Zn ₃	C ₁₅ H ₃₃ F ₆ N ₄ O ₃ PZn
<i>a</i> = ... (esd) Å	8.2471(9)	9.565(3)	9.5547(7)	9.0397(8)	7.2751(5)	8.7520(10)	25.8872(12)
<i>b</i> = ... (esd) Å	13.794(2)	14.488(3)	14.1978(7)	30.477(3)	27.652(2)	9.3289(10)	25.8872(12)
<i>c</i> = ... (esd) Å	15.1499(17)	14.644(4)	14.4613(10)	8.9610(8)	9.5242(7)	14.889(2)	17.1214(8)
<i>a</i> = ... (esd) °	90	90	90	90	90	72.755(10)	90
<i>β</i> = ... (esd) °	95.689(9)	92.30(2)	92.613(6)	94.189(8)	106.512(6)	89.362(10)	90
<i>γ</i> = ... (esd) °	90	90	90	90	90	63.372(8)	120
<i>V</i> = ... Å ³	1715.0(4)	2027.6(9)	1973.3(2)	2189.8(4)	1837.0(2)	1027.2(2)	9936.6(10)
<i>Z</i> =	4	4	4	4	4	1	18
Formula weight	366.23	511.20	515.19	556.25	410.86	966.68	527.79
Space group	<i>P</i> 2 ₁ / <i>c</i>	<i>P</i> 2 ₁ / <i>c</i>	<i>P</i> 2 ₁ / <i>c</i>	<i>P</i> 2 ₁ / <i>n</i>	<i>P</i> 2 ₁ / <i>n</i>	<i>P</i> 1	<i>R</i> 3 <i>c</i>
<i>T</i> = ... °C	150(2)	150(2)	150(2)	150(2)	150(2)	150(2)	150(2)
<i>λ</i> = ... Å	0.71073	0.71073	0.71073	0.71073	0.71073	0.71073	0.71073
<i>D</i> _{calcd} = ... g cm ^{−3}	1.418	1.675	1.734	1.687	1.486	1.563	1.588
<i>μ</i> = ... mm ^{−1}	1.078	1.054	1.283	1.164	1.491	2.166	1.259
<i>R</i> ₁ (<i>F</i> _o ²) =	0.0523	0.0819	0.0451	0.0508	0.0629	0.1012	0.0429
<i>wR</i> ₂ (<i>F</i> _o ²) =	0.1417	0.2704	0.1212	0.1160	0.1700	0.2773	0.1106

$$^a R_1 = \sum |F_o| - |F_c| / \sum |F_o|; wR_2 = \{ \sum [w(F_o^2 - F_c^2)]^2 \}^{1/2}$$

Table 2 Selected bond lengths [Å] and angles [°]

Mn(Me ₂ B13N4)Cl ₂		
Mn(1)–N(4)	2.317(3)	
Mn(1)–N(1)	2.320(3)	
Mn(1)–N(3)	2.324(3)	
Mn(1)–N(2)	2.331(3)	
Mn(1)–Cl(2)	2.4396(9)	
Mn(1)–Cl(1)	2.4559(9)	
N(4)–Mn(1)–N(1)	81.97(9)	
N(4)–Mn(1)–N(3)	78.47(9)	
N(1)–Mn(1)–N(3)	74.92(9)	
N(4)–Mn(1)–N(2)	150.29(10)	
N(1)–Mn(1)–N(2)	78.98(10)	
N(3)–Mn(1)–N(2)	74.70(10)	
N(4)–Mn(1)–Cl(2)	99.12(7)	
N(1)–Mn(1)–Cl(2)	92.48(7)	
N(3)–Mn(1)–Cl(2)	167.36(7)	
N(2)–Mn(1)–Cl(2)	104.25(8)	
N(4)–Mn(1)–Cl(1)	99.79(7)	
N(1)–Mn(1)–Cl(1)	168.38(7)	
N(3)–Mn(1)–Cl(1)	94.10(7)	
N(2)–Mn(1)–Cl(1)	94.65(8)	
Cl(2)–Mn(1)–Cl(1)	98.54(4)	
[Mn(Me ₂ B13N4)Cl ₂] ₂ PF ₆		
Mn(1)–N(3)	2.093(12)	
Mn(1)–N(1)	2.100(12)	
Mn(1)–Cl(2)	2.250(4)	
Mn(1)–Cl(1)	2.266(5)	
Mn(1)–N(4)	2.275(12)	
Mn(1)–N(2)	2.296(10)	
N(3)–Mn(1)–N(1)	83.3(4)	
N(3)–Mn(1)–Cl(2)	93.2(3)	
N(1)–Mn(1)–Cl(2)	176.5(4)	
N(3)–Mn(1)–Cl(1)	173.8(3)	
N(1)–Mn(1)–Cl(1)	93.1(3)	
Cl(2)–Mn(1)–Cl(1)	90.43(16)	
N(3)–Mn(1)–N(4)	90.8(5)	
N(1)–Mn(1)–N(4)	81.8(4)	
Cl(2)–Mn(1)–N(4)	98.1(4)	
Cl(1)–Mn(1)–N(4)	93.6(4)	
N(3)–Mn(1)–N(2)	81.7(4)	
N(1)–Mn(1)–N(2)	77.2(4)	
Cl(2)–Mn(1)–N(2)	102.6(3)	
Cl(1)–Mn(1)–N(2)	92.6(3)	
N(4)–Mn(1)–N(2)	158.3(4)	
[Co(Me ₂ B13N4)Cl ₂] ₂ PF ₆ ·CH ₃ CN		
Cl(1)–Co(1)	2.2859(17)	
Cl(2)–Co(1)	2.2541(19)	
Co(1)–N(1)	1.956(5)	
Co(1)–N(3)	1.988(5)	
Co(1)–N(2)	2.029(5)	
Co(1)–N(4)	2.047(4)	
N(1)–Co(1)–N(3)	88.1(2)	
N(1)–Co(1)–N(2)	83.6(2)	
N(3)–Co(1)–N(2)	85.9(2)	
N(1)–Co(1)–N(4)	87.7(2)	
N(3)–Co(1)–N(4)	92.4(2)	
N(2)–Co(1)–N(4)	171.2(2)	
N(1)–Co(1)–Cl(2)	179.14(15)	
N(3)–Co(1)–Cl(2)	92.43(16)	
N(2)–Co(1)–Cl(2)	97.09(15)	
N(4)–Co(1)–Cl(2)	91.64(15)	
N(1)–Co(1)–Cl(1)	91.04(15)	
N(3)–Co(1)–Cl(1)	173.01(15)	
N(2)–Co(1)–Cl(1)	87.07(15)	
N(4)–Co(1)–Cl(1)	94.54(14)	
Cl(2)–Co(1)–Cl(1)	88.46(6)	
[Co(Me ₂ B13N4)Cl ₂] ₂ PF ₆		
Co(1)–N(1)	1.954(2)	
Co(1)–N(3)	1.998(2)	
Co(1)–N(2)	2.035(3)	
Co(1)–N(4)	2.055(3)	

Table 2 (Contd.)

[Co(Me ₂ B13N4)Cl ₂] ₂ PF ₆		
Co(1)–Cl(2)	2.2509(8)	
Co(1)–Cl(1)	2.2785(8)	
N(1)–Co(1)–N(3)	88.10(10)	
N(1)–Co(1)–N(2)	83.13(11)	
N(3)–Co(1)–N(2)	86.42(11)	
N(1)–Co(1)–N(4)	87.46(11)	
N(3)–Co(1)–N(4)	92.91(11)	
N(2)–Co(1)–N(4)	170.59(10)	
N(1)–Co(1)–Cl(2)	179.11(8)	
N(3)–Co(1)–Cl(2)	91.78(7)	
N(2)–Co(1)–Cl(2)	97.74(8)	
N(4)–Co(1)–Cl(2)	91.66(8)	
N(1)–Co(1)–Cl(1)	92.41(8)	
N(3)–Co(1)–Cl(1)	173.42(8)	
N(2)–Co(1)–Cl(1)	87.13(8)	
N(4)–Co(1)–Cl(1)	93.67(8)	
Cl(2)–Co(1)–Cl(1)	87.81(3)	
[Cu(Me ₂ B13N4)Cl] ₂ ·2H ₂ O		
Cu(1)–N(1)	2.046(4)	
Cu(1)–N(2)	2.048(3)	
Cu(1)–N(4)	2.073(4)	
Cu(1)–N(3B)	2.118(10)	
Cu(1)–N(3A)	2.238(10)	
Cu(1)–Cl(1)	2.2645(12)	
N(1)–Cu(1)–N(2)	85.60(14)	
N(1)–Cu(1)–N(4)	84.72(16)	
N(2)–Cu(1)–N(4)	169.88(15)	
N(1)–Cu(1)–N(3B)	85.6(3)	
N(2)–Cu(1)–N(3B)	98.0(3)	
N(4)–Cu(1)–N(3B)	84.2(3)	
N(1)–Cu(1)–N(3A)	82.1(3)	
N(2)–Cu(1)–N(3A)	87.1(2)	
N(4)–Cu(1)–N(3A)	94.4(2)	
N(1)–Cu(1)–Cl(1)	168.40(12)	
N(2)–Cu(1)–Cl(1)	94.01(11)	
N(4)–Cu(1)–Cl(1)	94.87(12)	
N(3B)–Cu(1)–Cl(1)	105.9(2)	
N(3A)–Cu(1)–Cl(1)	109.5(2)	
[Zn(Me ₂ B13N4)Cl(H ₂ O)] ₂ [ZnCl ₄]·CH ₃ CN		
Zn(1)–N(3)	2.15(3)	
Zn(1)–N(1)	2.15(3)	
Zn(1)–N(4)	2.16(3)	
Zn(1)–O(1)	2.20(2)	
Zn(1)–N(2)	2.26(3)	
Zn(1)–Cl(1)	2.362(10)	
N(3)–Zn(1)–N(1)	82.1(11)	
N(3)–Zn(1)–N(4)	93.0(11)	
N(1)–Zn(1)–N(4)	84.9(11)	
N(3)–Zn(1)–O(1)	171.1(11)	
N(1)–Zn(1)–O(1)	94.7(10)	
N(4)–Zn(1)–O(1)	95.1(11)	
N(3)–Zn(1)–N(2)	81.4(10)	
N(1)–Zn(1)–N(2)	78.7(10)	
N(4)–Zn(1)–N(2)	163.2(10)	
O(1)–Zn(1)–N(2)	89.8(10)	
N(3)–Zn(1)–Cl(1)	97.5(7)	
N(1)–Zn(1)–Cl(1)	178.3(8)	
N(4)–Zn(1)–Cl(1)	96.8(8)	
O(1)–Zn(1)–Cl(1)	85.5(7)	
N(2)–Zn(1)–Cl(1)	99.6(7)	
Zn(2)–N(7)	2.12(3)	
Zn(2)–O(2)	2.13(3)	
Zn(2)–N(8)	2.16(2)	
Zn(2)–N(5)	2.19(3)	
Zn(2)–N(6)	2.24(3)	
Zn(2)–Cl(2)	2.387(8)	
N(7)–Zn(2)–O(2)	169.6(10)	
N(7)–Zn(2)–N(8)	94.0(11)	
O(2)–Zn(2)–N(8)	95.8(10)	
N(7)–Zn(2)–N(5)	82.5(11)	
O(2)–Zn(2)–N(5)	95.0(10)	
N(8)–Zn(2)–N(5)	84.3(10)	

Table 2 (Contd.)

$[\text{Zn}(\text{Me}_2\text{B13N4})\text{Cl}(\text{H}_2\text{O})]_2[\text{ZnCl}_4]\cdot\text{CH}_3\text{CN}$	
N(7)–Zn(2)–N(6)	82.1(10)
O(2)–Zn(2)–N(6)	87.5(9)
N(8)–Zn(2)–N(6)	162.1(9)
N(5)–Zn(2)–N(6)	77.8(9)
N(7)–Zn(2)–Cl(2)	95.6(8)
O(2)–Zn(2)–Cl(2)	86.5(6)
N(8)–Zn(2)–Cl(2)	98.0(7)
N(5)–Zn(2)–Cl(2)	177.1(8)
N(6)–Zn(2)–Cl(2)	99.8(7)
$[\text{Zn}(\text{Me}_2\text{B13N4})(\text{OAc})(\text{H}_2\text{O})]\text{PF}_6$	
N(1)–Zn(1)	2.151(5)
N(2)–Zn(1)	2.143(4)
N(3)–Zn(1)	2.222(5)
N(4)–Zn(1)	2.138(4)
O(2)–Zn(1)	2.034(4)
Zn(1)–O(1)	2.152(4)
O(2)–Zn(1)–N(4)	90.98(16)
O(2)–Zn(1)–N(2)	174.50(17)
N(4)–Zn(1)–N(2)	83.52(18)
O(2)–Zn(1)–N(1)	96.83(18)
N(4)–Zn(1)–N(1)	91.7(2)
N(2)–Zn(1)–N(1)	83.3(2)
O(2)–Zn(1)–O(1)	89.52(15)
N(4)–Zn(1)–O(1)	169.13(19)
N(2)–Zn(1)–O(1)	95.90(17)
N(1)–Zn(1)–O(1)	99.01(19)
O(2)–Zn(1)–N(3)	99.07(18)
N(4)–Zn(1)–N(3)	83.3(2)
N(2)–Zn(1)–N(3)	80.46(19)
N(1)–Zn(1)–N(3)	163.41(19)
O(1)–Zn(1)–N(3)	85.86(18)

Descriptions of specific structures

$[\text{Mn}(\text{Me}_2\text{B13N4})\text{Cl}_2]$ occurs as discrete complexes in the solid state featuring a distorted octahedral coordination about the Mn^{2+} ion (Fig. 4). As is the case for all of the 6-coordinate examples described here, the complex adopts the *cis*-V configuration with metal residing in the pocket of the ligand and the two remaining coordination site *cis* to each other.

$[\text{Mn}(\text{Me}_2\text{B13N4})\text{Cl}_2]\text{PF}_6$ (Fig. 5) is similar to the analogous Mn^{2+} complex in many ways, but with contracted Mn–N bond lengths and altered bond angles appropriate to the smaller Mn^{3+} cation. The cobalt analogue, $[\text{CoMe}_2\text{B13N4Cl}_2]\text{PF}_6$

obtained as green hexagonal plates, is isostructural with the manganese compound, but there are small differences in the coordination geometry about the metal ion, which are discussed later.

A second form of the Co^{3+} complex was obtained as green needles. This was shown by X-ray diffraction to be the solvate $[\text{Co}(\text{Me}_2\text{B13N4})\text{Cl}_2]\text{PF}_6\cdot\text{MeCN}$ (Fig. 6). The asymmetric unit contains a single $[\text{Co}(\text{Me}_2\text{B13N4})\text{Cl}_2]^+$ ion, two half PF_6^- anions and one well-determined molecule of acetonitrile. The coordination about the metal is not significantly altered by this but the packing is different.

$[\text{Cu}(\text{Me}_2\text{B13N4})\text{Cl}]\text{Cl}\cdot 2\text{H}_2\text{O}$ is the only structure here to feature unbound chloride (Fig. 7). This a reflection of the greater reluctance of Cu^{2+} to adopt (undistorted) octahedral geometry compared with the other ions. The copper ion is five coordinate in an arrangement similar to the other complexes here, but with apparently one coordinating chloride removed. The result is a slightly distorted square pyramidal coordination about Cu^{2+} ($4 \times \text{N}$, $1 \times \text{Cl}$).

Crystallographically, this structure is intriguing because of the disorder within the $\text{Me}_2\text{B13N4}$ macrocycle which adopts two different orientations depending on the location of the propylene bridge. The crystal is not “bad” – the disorder is a reflection that the energies for packing each of the two different forms in the solid are very similar. Fig. 8 below shows the complete model, with each of the two components highlighted in red. Note the difference in the carbon atom positions.

The structure of $[\text{Zn}(\text{Me}_2\text{B13N4})\text{Cl}(\text{OH}_2)]_2[\text{ZnCl}_4]\cdot\text{CH}_3\text{CN}$ is non-centrosymmetric and contains four symmetry unique components: two independent $[\text{Zn}(\text{Me}_2\text{B13N4})\text{Cl}(\text{OH}_2)]^+$ ions, a tetrahedral $[\text{ZnCl}_4]^{2-}$ ion, and one molecule of acetonitrile (Fig. 9). The two $[\text{Zn}(\text{Me}_2\text{B13N4})\text{Cl}(\text{OH}_2)]^+$ ions each adopt a similar coordination geometry to the other octahedral ions described here, with the macrocycle tetradentate to Zn^{2+} and water and chloride completing the coordination in a *cis* arrangement. These two symmetry-unique $[\text{Zn}(\text{Me}_2\text{B13N4})\text{Cl}(\text{OH}_2)]^+$ ions form a hydrogen-bonded dimer through $\text{O}\cdots\text{H}\cdots\text{Cl}$ interactions that is approximately centrosymmetric. There are no intramolecular $\text{O}\cdots\text{H}\cdots\text{Cl}$ hydrogen bonds but

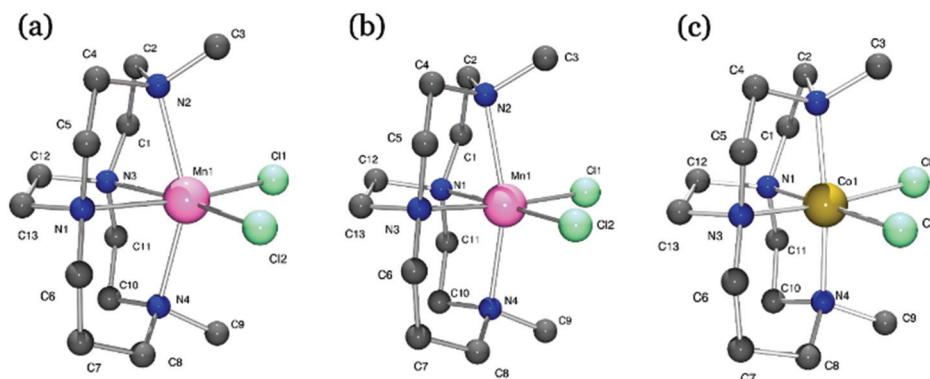


Fig. 3 X-ray crystal structures of (a) $\text{Mn}(\text{Me}_2\text{B13N4})\text{Cl}_2$ (b) $\text{Mn}(\text{Me}_2\text{B13N4})\text{Cl}_2^+$ and (c) $\text{Co}(\text{Me}_2\text{B13N4})\text{Cl}_2^+$ (green block, without CH_3CN).

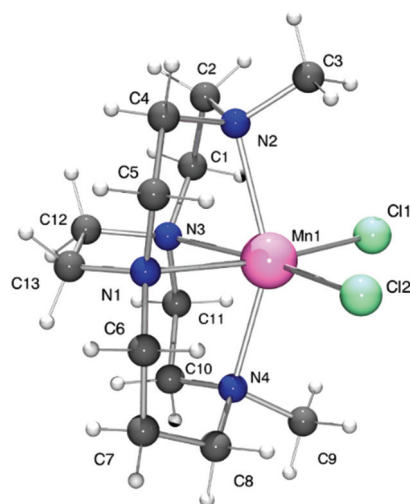


Fig. 4 Crystal structure of $[\text{Mn}(\text{Me}_2\text{B13N4})\text{Cl}_2]$.

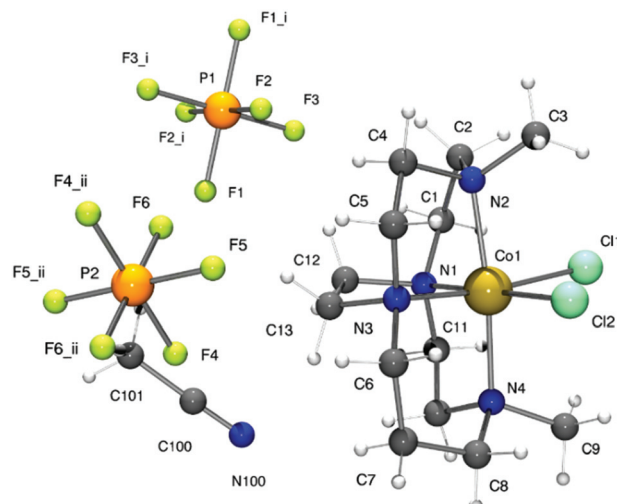


Fig. 6 Representation of the molecular units within $[\text{Co}(\text{Me}_2\text{B13N4})\text{Cl}_2] \cdot \text{PF}_6 \cdot \text{MeCN}$. Symmetry equivalent atoms are generated by the operators: $i = 1 - x, -y, 1 - z$; $ii = 2 - x, -y, -z$.

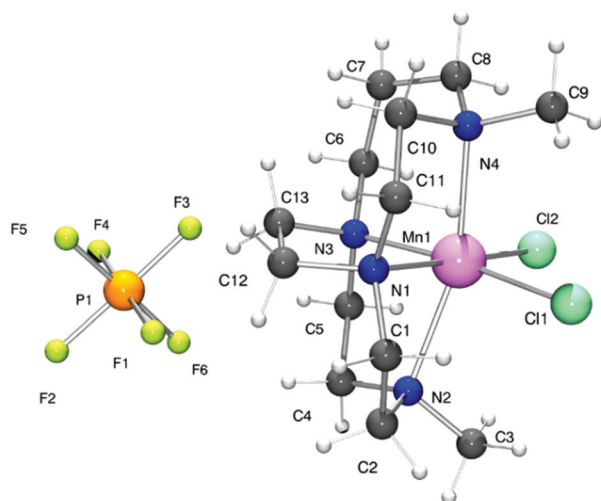


Fig. 5 Crystal structure of $[\text{Mn}(\text{Me}_2\text{B13N4})\text{Cl}_2]\text{PF}_6$.

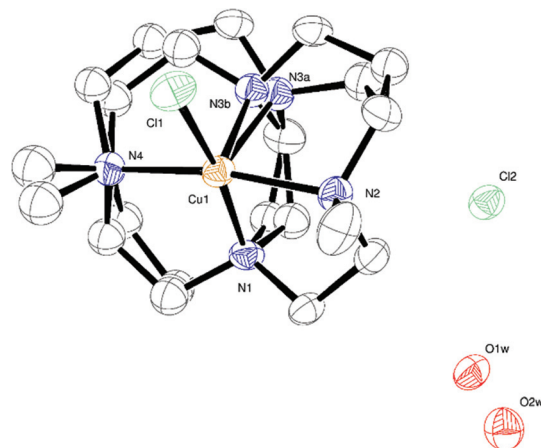


Fig. 7 Complete asymmetric unit for $[\text{Cu}(\text{Me}_2\text{B13N4})\text{Cl}]\text{Cl} \cdot 2\text{H}_2\text{O}$. Atoms are drawn as 50% probability ellipsoids. Hydrogen atoms have been omitted for clarity.

each bound water forms a second interaction: O1–H1C forms a hydrogen bond to N100 (acetonitrile) and O2–H2D forms a hydrogen bond to the $[\text{ZnCl}_4]^{2-}$ ion.

For $[\text{Zn}(\text{Me}_2\text{B13N4})\text{OAc}(\text{OH}_2)]\text{PF}_6$, the use of zinc acetate rather than zinc chloride leads to a different ligand set about the zinc ion (Fig. 10). The macrocycle is tetradentate to octahedral Zn^{2+} and the coordination is completed by *cis* water and acetate. Charge balancing is completed by the PF_6^- anion. The structure contains intramolecular and intermolecular hydrogen bonds involving bound water and acetate. There is an intramolecular hydrogen bond between O3 and H1C (O3...O1 distance is 2.669(6) Å). Hydrogen-bonded trimers of $[\text{Zn}(\text{Me}_2\text{B13N4})\text{OAc}(\text{OH}_2)]^+$ are formed from three symmetry-equivalent complexes held together by O–H...O interactions (Fig. 11).

Kinetic stability of $[\text{Cu}(\text{Me}_2\text{B13N4})\text{Cl}]\text{Cl}$

Cross-bridged tetraazamacrocyclic complexes typically gain stability compared to unbridged analogues under harsh conditions due to their topological complexity and the rigidity caused by their small size.^{18–20,31} Yet, the proton-sponge basicity of many of these ligands precludes aqueous titration in the presence of metal ions to produce formation constants. As an alternative, kinetic decomplexation studies using high acid concentration under pseudo first order conditions are used to give some quantification of complex stability. Typically, only copper(II) complexes are subjected to these studies and have yielded published data for comparison. They are often the first (or only) transition metal complex synthesized due to the interest in PET imaging applications of ^{64}Cu . Weisman has standar-

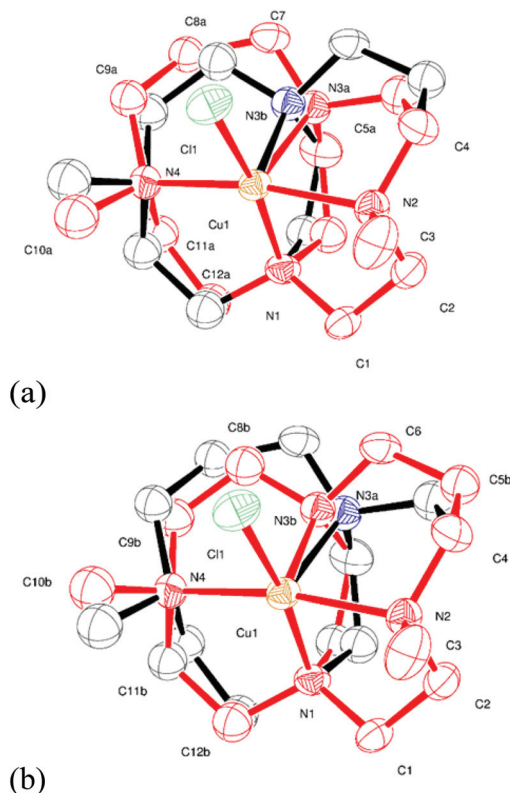


Fig. 8 (a) Component 1 of the macrocycle shown in red (b) component 2 of the macrocycle shown in red.

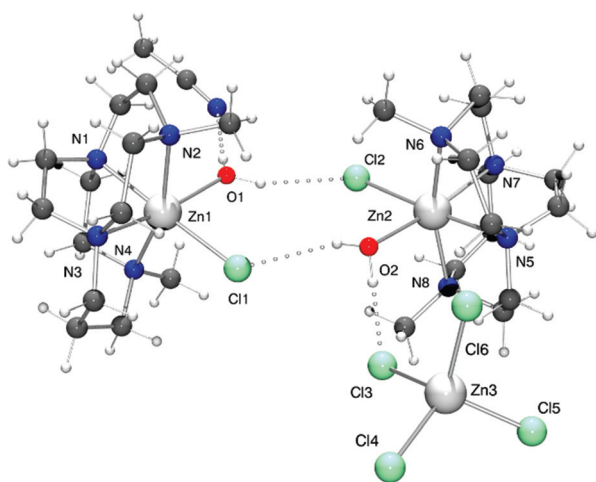


Fig. 9 Crystal structure of $[\text{Zn}(\text{Me}_2\text{B13N4})\text{Cl}(\text{OH}_2)]_2[\text{ZnCl}_4] \cdot \text{CH}_3\text{CN}$. Dashed lines are hydrogen bonds.

dized^{9,11,13,15} probing the stability of new cross-bridged ligands using the copper(II) complex. Although established by Busch^{17,18} using different conditions, Weisman has chosen 5 M HCl and various temperature points, such as 30 °C, 50 °C, and 90 °C as benchmarks for kinetic stability of new Cu cross-bridged complexes.

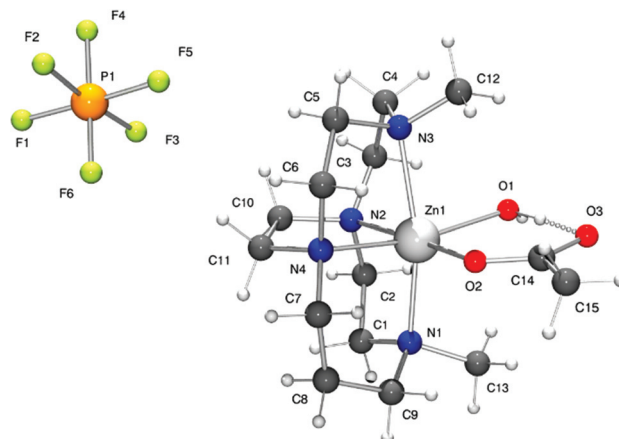


Fig. 10 Crystal structure of $[\text{Zn}(\text{Me}_2\text{B13N4})\text{OAc}(\text{OH}_2)]\text{PF}_6$.

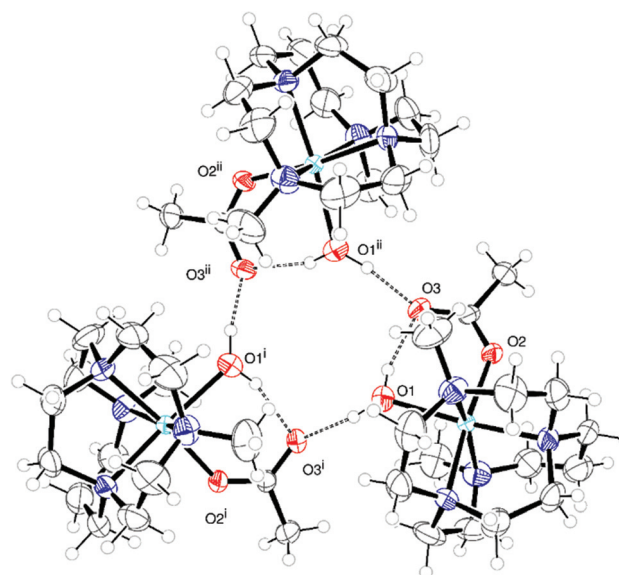


Fig. 11 Intramolecular and intermolecular hydrogen bonding in $[\text{Zn}(\text{Me}_2\text{B13N4})\text{OAc}(\text{OH}_2)]\text{PF}_6$. Dashed lines show hydrogen bonds.

Results of the decomplexation studies of $[\text{Cu}(\text{Me}_2\text{B13N4})\text{Cl}]\text{Cl}$ and related complexes are presented in Table 4.

One major trend easily visible in the kinetic stability data is the increased kinetic stability towards strong acid decomplexation with increased macrocycle ring size. The cyclam based complexes are stable in 5 M HCl at 90 °C with measurable half-lives. The **Me₂B13N4** ligand which is the subject of this work gave a half-life under these conditions of approximately 2 minutes, which was just at the edge of what was measurable with our instrumentation. We did not attempt this temperature with the cyclen based complexes at this temperature since they gave half-lives that were not measurable at the lower temperature of 50 °C with 5 M HCl. Clearly the smallest cyclen cross-bridged tetraazamacrocycles do not provide a complementary size/geometry match for Cu^{2+} to withstand these

Table 3 Comparison of $N_{ax}-M-N_{ax}$ and $N_{eq}-M-N_{eq}$ bond angles across metal ions of differing ionic radius and ethylene cross-bridged tetraaza-macrocycles of differing size^a

Metal ion	H.S. 6-coord. ionic radius	Me₂EBC		Ref.	Me₂B13N4 (this work)		Me₂Bcyclen		Ref.
		$N_{ax}-M-N_{ax}$	$N_{eq}-M-N_{eq}$		$N_{ax}-M-N_{ax}$	$N_{eq}-M-N_{eq}$	$N_{ax}-M-N_{ax}$	$N_{eq}-M-N_{eq}$	
Mn ²⁺	97	158.0(2)	75.6(2)	18	150.29(10)	74.92(9)	144.0(2)	74.1(2)	18
Fe ²⁺	92	161.88(5)	78.36(5)	18	—	—	145.78(7)	77.31(7)	18
Co ²⁺	89	172.4(2)	81.11(13)	35	—	—	149.81(9)	80.86(8)	35
Zn ²⁺	88	—	—	—	163.41(19) ^b	83.52(18) ^b	150.75(7)	78.32(7)	37
Ni ²⁺	83	174.56(10) ^c	85.07(9) ^c	36	—	—	161.58(13) ^c	85.46(13) ^c	36
Cu ²⁺	79 ^d	175.16(13) ^d	85.30(12) ^d	41	169.88(15) ^d	82.1(3) ^d	164.85(13) ^e	83.92(14) ^e	37
Mn ³⁺	79	170.1(2)	81.7(2)	42	158.3(4)	83.3(4)	155.01(11)	81.29(11)	42
Fe ³⁺	79	—	—	—	—	—	153.20(9)	77.81	43
Cr ³⁺	76	172.46(11)	84.63(11)	44	—	—	160.83(19)	83.50(18)	44
Cr ³⁺	76	171.44(14)	84.18(13)	45	—	—	161.62(11)	83.23(10)	45
Co ³⁺	75	—	—	—	170.59(10)	88.10(10)	168.8(4)	87.2(4)	35
					171.2(2)	88.1(2)			

^a Complex is $MLCl_2^{n+}$ unless otherwise designated. ^b $Zn(L)(OAc)(OH_2)^+$. ^c $Ni(L)(acac)^+$. ^d Ionic radius and bond angles are for 5-coord complex $Cu(L)Cl^+$. ^e $Cu(L)(NCCH_3)_2$.

Table 4 Half-lives of selected copper(II) complexes in HCl

Ligand	30 °C 1 M HCl	40 °C 1 M HClO ₄	50 °C 5 M HCl	90 °C 5 M HCl	Ref.
H ₂ Bcyclen	<1 min	—	<1 min	—	^a
Me ₂ Bcyclen	36 min	30 h	<1 min	—	37 ^a
H ₂ B13N4	4.8 hour	—	—	—	15,46
Me ₂ B13N4	7.7 day	—	30.1 min	<2 min	^a
H ₂ EBC	—	—	—	11.8 min	9
Me ₂ EBC	—	>6 years	7.3 day	79 min	37,47

^a This work.

harsh conditions, which can also be seen in the X-ray crystal structural data given in highly distorted bond angles of Table 3. There is an impressive amount of stability gained by adding just one ($-CH_2-$) to the size of the parent macrocycle for the dimethyl complexes: 7.7 days vs. 36 minutes for Cu-**Me₂B13N4** vs. Cu-**Me₂Bcyclen** at 30 °C in 1 M HCl, suggesting modest gains in bond angles (see Table 3) can yield important amounts of complex stability due to increased complementarity.

A second clear trend is the advantage in stability gained by the dimethyl ligands over the dihydro ligands. For example, **Me₂EBC** at 90 °C in 5 M HCl gave a half-life for its Cu²⁺ complex of 79 minutes, while the Cu-**H₂EBC** complex is reported to have a half-life under the same conditions of just 11.8 minutes.⁹ The smaller, less stable ligand complexes tested at 30 °C in 1 M HCl demonstrated a similar trend. Cu-**Me₂B13N4** had an impressive half-life under these conditions of 7.7 days, while Cu-**H₂B13N4** gave a half-life of only 4.8 hours.^{15,46} Cu-**Me₂Bcyclen** gave a half-life of 36 minutes under these conditions, while Cu-**H₂Bcyclen** had a half-life too short to be measure and thus is listed as less than 1 minute. Interestingly, 7.7 days is 38.5 times longer than 4.8 hours, approximately the same fold gain in stability as seen in the

36 minute vs. <1 minute half-life for Cu-**Me₂Bcyclen** and Cu-**H₂Bcyclen**, respectively. Making all nitrogen donors tertiary increases the rigidity of the ligand and provides some steric protection of the nitrogen atom from protons in solution, slowing down protonation, and thus decomplexation. The dihydro ligands have secondary nitrogen atoms with ionizable hydrogen atoms that easily exchange with protons in solution, providing for much faster interaction with the highly acidic solution and as demonstrated, faster decomplexation under strong acid conditions.

Finally, there appears to be some role for the chloride of HCl in the decomplexation of the copper complexes as well. The original acid decomplexation of cross-bridged tetraaza-macrocyclic copper complexes³⁷ used 1 M HClO₄ at 40 °C to determine how stable these complexes were. Cu-**Me₂EBC** gave a half-life estimated at >6 years and Cu-**Me₂Bcyclen** gave a half-life of 30 h under these conditions. Due to the extreme stability of Cu-**Me₂EBC**, we did not attempt to repeat this experiment at 30 °C in 1 M HCl, but we did carry out this experiment for Cu-**Me₂Bcyclen**. At the same H⁺ concentration and 10 °C lower temperature, the half-life in HCl was found to be only 36 minutes, much shorter than the 30 hours in 1 HClO₄ at 40 °C. Since Cl[−] is a coordinating anion and is found bound to the metal ions in many of the crystal structures in Table 3, its involvement in the decomplexation process should perhaps be expected. Typically non-coordinating ClO₄[−] is less likely to interact with the metal complex. Clearly, choice of which strong acid to use in these decomplexation experiments can make a significant difference in the resulting half-lives.

Electronic characterization of iron and manganese complexes

We have previously published the synthesis and characterization of cobalt,³⁵ nickel,³⁶ copper,³⁷ and zinc³⁷ complexes of **Me₂B13N4** except for the X-ray crystal structures presented above. However, the iron and manganese complexes synthesized for this study are novel and are of interest to us as

potential oxidation catalysts. We have synthesized them initially in their divalent forms from the corresponding chloride metal salt, and then oxidized them to the trivalent oxidation state using molecular bromine as the oxidant. Here, we present characterization of the electronic structure of these species prior to, and as a way to help understand, the oxidation screening experiments that will conclude this work.

The magnetic moments of the solid state divalent and trivalent iron and manganese complexes were determined in order to probe the high spin or low spin nature of the complexes, and thus indicate the relative ligand field strength. The divalent species were air sensitive, so they were introduced into the sample tube in an inert atmosphere glovebox and the tubes sealed with a septum prior to taking the measurements. All four complexes $\text{Fe}(\text{Me}_2\text{B13N4})\text{Cl}_2$, $\text{Mn}(\text{Me}_2\text{B13N4})\text{Cl}_2$, $[\text{Fe}(\text{Me}_2\text{B13N4})\text{Cl}_2]\text{PF}_6$, and $[\text{Mn}(\text{Me}_2\text{B13N4})\text{Cl}_2]\text{PF}_6$ gave values (see Experimental section) consistent with high spin behavior, as was observed for their previously published analogues with the **Me₂Bcyclen** and **Me₂EBC** ligands.^{18,42,48} This is consistent with the relatively weak field folded tetraazamacrocyclic ligands used in these studies.

The electronic spectra of all four iron and manganese complexes of **Me₂B13N4** were obtained in acetonitrile. The Experimental section contains the absorbances and extinction coefficients. As expected for high spin d^5 and d^6 complexes with ligands of this type,⁴⁹ neither divalent complex exhibit intense spectral features, except for tailing absorbances at highest energy. $\text{Fe}(\text{Me}_2\text{B13N4})\text{Cl}_2$ does have one discernable peak with $\lambda_{\text{max}} = 342 \text{ nm}$ ($\epsilon = 623 \text{ M}^{-1} \text{ cm}^{-1}$) most likely to be of a low energy charge transfer nature. Similar absorbances were observed for $\text{Fe}(\text{Me}_2\text{EBC})\text{Cl}_2$ and $\text{Fe}(\text{Me}_2\text{Bcyclen})\text{Cl}_2$.¹⁸

Me₂B13N4 in acetonitrile. The high spin $d^5 \text{ Fe}^{3+}$ spectrum of $[\text{Fe}(\text{Me}_2\text{B13N4})\text{Cl}_2]\text{PF}_6$ and the high spin $d^4 \text{ Mn}^{3+}$ spectrum of $[\text{Mn}(\text{Me}_2\text{B13N4})\text{Cl}_2]\text{PF}_6$ in acetonitrile were obtained. Both metal ions have several charge transfer bands, with the iron(III) complex having no other absorptions, which is similar to both $[\text{Fe}(\text{Me}_2\text{EBC})\text{Cl}_2]\text{PF}_6$ and $[\text{Fe}(\text{Me}_2\text{Bcyclen})\text{Cl}_2]\text{PF}_6$.⁴² However, the manganese(III) complex also has two low energy bands typical of this ion.⁴⁹ These bands are fairly intense for d-d transitions, are characteristically broad, and may result from electronic transitions involving the tetragonally split $^5\text{B}_{1g}(\text{E}_g)$ and $^5\text{B}_{2g}(\text{T}_{2g})$ states.⁴⁹ Both $[\text{Mn}(\text{Me}_2\text{EBC})\text{Cl}_2]\text{PF}_6$ and $[\text{Mn}(\text{Me}_2\text{Bcyclen})\text{Cl}_2]\text{PF}_6$ gave similar low energy electronic absorptions.⁴² Interestingly, these previously published complexes only gave one d-d transition at 534 nm ($540 \text{ M}^{-1} \text{ cm}^{-1}$) and 530 nm ($190 \text{ M}^{-1} \text{ cm}^{-1}$), respectively, whereas the present **Me₂B13N4** complex has a similar absorption at 526 nm ($512 \text{ M}^{-1} \text{ cm}^{-1}$). But it also shows another shoulder at 400 nm ($960 \text{ M}^{-1} \text{ cm}^{-1}$) that was not observable for the cyclam and cyclen derivative. Perhaps the less symmetric **Me₂B13N4** ligand allows observation of this additional peak.

Electrochemistry

$\text{Mn}(\text{Me}_2\text{EBC})\text{Cl}_2$,^{17–30,32,33} $\text{Fe}(\text{Me}_2\text{EBC})(\text{OTf})_2$,⁵⁰ and $\text{Me}(\text{Me}_2\text{Bcyclen})\text{Cl}_2$ ³⁴ have all been established as oxidation catalysts with varying degrees of detail about their respective oxidation

Table 5 Redox potential versus SHE for MnCl_2 and FeCl_2 complexes of **Me₂EBC**, **Me₂Bcyclen**, and **Me₂B13N4**

Complex	$\text{M}^{2+/3+} E_{1/2} [\text{V}]$ ($\Delta E [\text{mV}]$)	$\text{M}^{3+/4+} E_{1/2} [\text{V}]$ ($\Delta E [\text{mV}]$)
$\text{Mn}(\text{Me}_2\text{Bcyclen})\text{Cl}_2$ ¹⁸	+0.466 (70)	+1.232 (102)
$\text{Mn}(\text{Me}_2\text{B13N4})\text{Cl}_2$	+0.526 (92)	+1.296 (95)
$\text{Mn}(\text{Me}_2\text{EBC})\text{Cl}_2$ ¹⁸	+0.585 (61)	+1.343 (65)
$\text{Fe}(\text{Me}_2\text{Bcyclen})\text{Cl}_2$ ¹⁸	+0.036 (64)	—
$\text{Fe}(\text{Me}_2\text{B13N4})\text{Cl}_2$	+0.076 (114)	—
$\text{Fe}(\text{Me}_2\text{EBC})\text{Cl}_2$ ¹⁸	+0.110 (63)	—

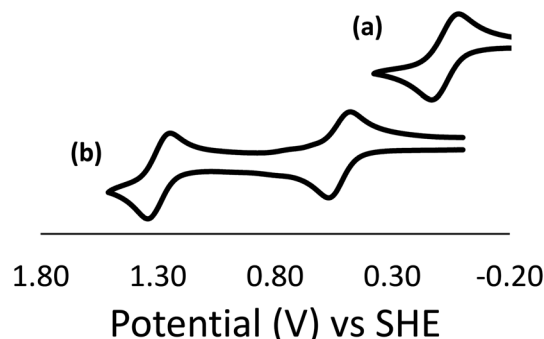


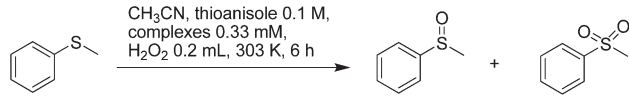
Fig. 12 Cyclic voltammograms in acetonitrile for (a) $\text{Fe}(\text{Me}_2\text{B13N4})\text{Cl}_2$ and (b) $\text{Mn}(\text{Me}_2\text{B13N4})\text{Cl}_2$.

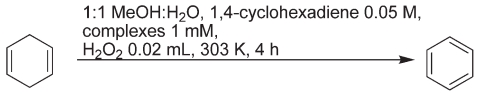
mechanisms known. Consistent with the need for stability of the catalyst at multiple oxidation states is the electrochemistry of these complexes, shown in Table 5.

We expected that if the cyclic voltammetry of the close analogues to these known oxidation catalysts, manganese(II) and iron(II) **Me₂B13N4**, gave similar results, that they too might be active oxidation catalyst. The results of the electrochemical study of these complexes are also listed in Table 5 and shown in Fig. 12, and fit exactly in the gaps between the **Me₂Bcyclen** and **Me₂EBC** complexes of a given metal ion. $\text{Mn}(\text{Me}_2\text{B13N4})\text{Cl}_2$ has a reversible $\text{Mn}^{2+/3+}$ couple at 0.526 V vs. SHE with $\Delta E = 92 \text{ mV}$ and a reversible $\text{Mn}^{3+/4+}$ couple at +1.296 V with $\Delta E = 95 \text{ mV}$. $\text{Fe}(\text{Me}_2\text{B13N4})\text{Cl}_2$ has a quasi-reversible $\text{Fe}^{2+/3+}$ couple at 0.076 V vs. SHE with $\Delta E = 114 \text{ mV}$. Based on the trends apparent in comparison with the other cross-bridged ligands, it appears that the redox potentials are closely tied to the ring size of the parent macrocycle. The smaller the ring size, the easier to oxidize the metal. As the higher oxidation state metal ion is smaller, it would fit the smaller ligand cavity better. The intermediate ring size of **Me₂B13N4** leads to intermediate redox potentials for both the manganese and iron complexes.

As observed for the **Me₂Bcyclen** and **Me₂EBC** complexes, the **Me₂B13N4** ligand stabilizes manganese in three oxidation states from $\text{Mn}^{2+}/\text{Mn}^{3+}/\text{Mn}^{4+}$ with good reversibility. Also similar to the other cross-bridged ligands, only Fe^{2+} and Fe^{3+} are observed in acetonitrile for $\text{Fe}(\text{Me}_2\text{B13N4})\text{Cl}_2$. Based on these experiments, we expected that $\text{Mn}(\text{Me}_2\text{B13N4})\text{Cl}_2$ would be the most likely candidate to perform well as an oxidation

Table 6 Oxidation catalysis screening results for manganese(II) and iron(II) complexes of **Me₂B13N4** in comparison to Mn(**Me₂EBC**)Cl₂ and Mn(**Me₂Bcyclen**)Cl₂

			
Complex	Conversion %	Yield % sulfoxide	Yield % sulfone
Mn(Me₂Bcyclen)Cl ₂	65.9	32.6	25.9
Mn(Me₂B13N4)Cl ₂	99.8	13.3	74.8
Mn(Me₂EBC)Cl ₂	99.8	44.3	46.5
Fe(Me₂B13N4)Cl ₂	28.8	18.1	4.4

		
Complex	Conversion %	Yield % benzene
Mn(Me₂Bcyclen)Cl ₂	88.0	51.2
Mn(Me₂B13N4)Cl ₂	74.1	63.1
Mn(Me₂EBC)Cl ₂	86.2	71.4
Fe(Me₂B13N4)Cl ₂	77.2	61.3

catalyst, due to the range of oxidations states that can be reversibly reached.

Catalytic oxidation studies

Iron and manganese bearing synthetic ligands generally have rich redox chemistry, and exploring their catalytic activity in oxidation catalysis is often fruitful. Herein, preliminary studies to investigate the divalent Mn and Fe **Me₂B13N4** complexes' activity in catalytic hydrogen abstraction and oxygen transfer were conducted using 1,4-cyclohexadiene and thioanisole as substrates with H₂O₂ oxidant, respectively.

As shown in Table 6, at 303 K, the Mn(**Me₂B13N4**)Cl₂ complex demonstrates high activity in sulfide oxidation. After 6 hours of reaction in acetonitrile, it provided almost complete conversion of thioanisole with 13.3% yield of sulfoxide and 74.8% of sulfone. Notably, compared with well-investigated Mn(**Me₂EBC**)Cl₂,^{17–30,32,33} and Mn(**Me₂Bcyclen**)Cl₂,³⁴ complexes which provided 99.8% and 65.9% conversion of sulfide with 44.3% and 32.6% of sulfoxide, 46.5% and 25.9% of sulfone, respectively, the Mn(**Me₂B13N4**)Cl₂ complex can more effectively oxidize sulfoxide to sulfone. This reactivity difference can't be solely assigned to the redox potential of the Mn^{III}/Mn^{IV} couple. As shown in Table 5, the potential of the Mn(**Me₂B13N4**)Cl₂ complex (+1.296 V vs. SHE) is higher than that of Mn(**Me₂Bcyclen**)Cl₂ (+1.232 V), but lower than the Mn(**Me₂EBC**)Cl₂ (+1.343 V), which should demonstrate the highest oxidizing power amongst its analogues.

Perhaps some combination of redox potential along with the steric and/or other electronic properties provided by the **Me₂B13N4** ligand are optimized for the production of sulfone. Another possibility is the involvement of the Mn^{2+/3+} couple in the mechanism of sulfoxide to sulfone oxidation. Mn-

(**Me₂B13N4**)Cl₂ has the intermediate redox potential not only of the Mn^{3+/4+} redox couple, but also of the Mn^{2+/3+} couple. Perhaps a value not too low and not too high, (a "Goldilocks" zone) is just right for sulfone production. Determination of these additional factors must await further in-depth mechanistic studies.

The Fe(**Me₂B13N4**)Cl₂ complex is sluggish in sulfide oxygenation, generating only 28.8% conversion of thioanisole with 18.1% yield of sulfoxide and 4.4% of the sulfone product. Its redox potential for the Fe^{II}/Fe^{III} couple is fairly low, +0.076 V vs. SHE, with no detected Fe^{III}/Fe^{IV} couple, which is consistent with the demonstrated low catalytic sulfide oxidation.

In hydrogen abstraction from 1,4-cyclohexadiene in methanol-water (1:1, v/v), Mn(**Me₂B13N4**)Cl₂ demonstrated more similar reactivity to its analogues, providing 74.1% conversion of substrate with 63.1% of the benzene product in 4 h at 303 K when using H₂O₂ as oxidant. Mn(**Me₂EBC**)Cl₂ gave 86.2% conversion with 71.4% yield, and Mn(**Me₂Bcyclen**)Cl₂ generated 51.2% yield of benzene with 88.0% conversion. In this reaction, the intermediate ligand size and redox potential of **Me₂B13N4** leads to the intermediate yield of benzene.

Although the manganese(IV) complex of the **Me₂B13N4** ligand has not been isolated yet, its manganese(IV) analogues, [Mn(**Me₂EBC**)(OH)₂](PF₆)₂ and [Mn(**Me₂Bcyclen**)(OH)₂](PF₆)₂ have been well characterized.^{22,34} Accordingly, having a similar ligand structure, a similar manganese(IV) species of the **Me₂B13N4** complex can be expected to occur under these oxidative conditions like its analogues, and is likely responsible for the hydrogen atom abstraction observed here.^{23,25}

Unlike in the sulfide oxidation, the Fe(**Me₂B13N4**)Cl₂ complex demonstrated comparable catalytic activity with its manganese(II) analogue, offering 77.2% conversion of 1,4-cyclohexadiene with 61.3% yield of benzene. The distinct reactivity of Fe(**Me₂B13N4**)Cl₂ complex in sulfide oxygenation and hydrogen abstraction has not been clarified yet, possibly related to its different mechanisms. One potential explanation is that, under the oxidative conditions with H₂O₂ oxidant, the iron(IV) species does not occur as suggested in the electrochemical studies (*vide supra*) because of the poor electron donation ability of **Me₂B13N4** ligand, thus the iron(III) species dominates in solution. Such an iron(III) species is very sluggish for oxygenation, but active for hydrogen abstraction for similar iron(III) species in lipooxygenases and their synthetic models.^{51,52} To our knowledge, the hydrogen atom abstraction ability of Fe(**Me₂EBC**)Cl₂ and Fe(**Me₂Bcyclen**)Cl₂ have not been published. It would be of interest to determine if these other low redox potential species are active hydrogen atom abstraction oxidation catalysts and to determine by what mechanism that reaction occurs if so.

Conclusions

Divalent and trivalent Mn and Fe complexes of **Me₂B13N4** were synthesized and characterized, both Mn complexes by X-ray crystallography. Five additional Co, Cu, and Zn

Me₂B13N4 structures were also presented, and in all seven structures **Me₂B13N4** binds the metal ion in a *cis*-V configuration of the homocyclen ring. Kinetic studies focusing on the decomposition of copper complexes in strong acid and at elevated temperatures show that the **Me₂B13N4** ligand releases Cu²⁺ much slower than either the smaller **Me₂Bcyclen** ligand or the **H₂B13N4** secondary nitrogen containing ligand. Further studies focused on the manganese and iron complexes as they were designed as potential oxidation catalysts. Solid state magnetic moment and acetonitrile solution electronic spectroscopy experiments revealed high spin, octahedral, metal complexes in all cases. Electrochemical studies of the divalent species under an inert atmosphere and in acetonitrile revealed reversible access to multiple oxidation states, a prerequisite for successful oxidation catalysis, in both cases. In particular, Mn(**Me₂B13N4**)Cl₂ was stabilized in Mn²⁺/Mn³⁺/Mn⁴⁺ oxidation states. Finally, preliminary screens for oxidation catalysis using H₂O₂ as the oxidant were carried out on the biomimetically important Mn and Fe complexes and showed promising results, particularly for Mn(**Me₂B13N4**)Cl₂, in the oxidation of thioanisole and for both Mn(**Me₂B13N4**)Cl₂ and Fe(**Me₂B13N4**)Cl₂ in the hydrogen atom abstraction of 1,4-cyclohexadiene. Future work will include expanding the range of oxidation reactions possible with these catalysts and determination of their oxidation catalysis mechanisms.

Experimental

General

Methyl iodide (99%), and sodium borohydride (98%), all anhydrous divalent transition metal salts, and all anhydrous solvents used in the glovebox were purchased from Aldrich Chemical Co. All other solvents were of reagent grade and were used without modification. 1,4,7,10-Tetraazacyclotridecane (homocyclen) was purchased from Strem Chemicals. *cis*-Decahydro-5*H*-2a,4a,7a,9a-tetraazacyclopenta[cd]phenalene (**1**) (homocyclen glyoxal) was prepared according to a literature method.¹⁵ Elemental analyses were performed by Quantitative Technologies Inc. Electrospray Mass spectra were collected on a Shimadzu LCMS-2020 instrument. All samples were dissolved in 50% H₂O/50% MeOH. Electron impact mass spectra were taken on solid samples using a Shimadzu QP2010S GCMS equipped with a direct insertion probe. NMR spectra were obtained on a Varian Bruker AVANCE II 300 MHz NMR Spectrometer. Electronic spectra were recorded using a Shimadzu UV-3600 UV-Vis-NIR Spectrophotometer. Magnetic moments were obtained on finely ground solid samples at ambient temperatures using a Johnson Matthey MSB Auto magnetic susceptibility balance. Electrochemical experiments were performed on a BAS Epsilon EC-USB Electrochemical Analyzer. A button Pt electrode was used as the working electrode with a Pt-wire counter electrode and a Ag-wire pseudo-reference electrode. Scans were taken at 200 mV s⁻¹. Acetonitrile solutions of the complexes (1 mM) with tetrabutylammonium hexafluorophosphate (0.1 M) as a supporting

electrolyte were used. The measured potentials were referenced to SHE using ferrocene (+0.400 V *versus* SHE) as an internal standard. All electrochemical measurements were carried out under N₂.

Ligand synthesis

Although we have published **Me₂B13N4** and **Me₂Bcyclen** complexes previously,^{35–37} only general syntheses following that of Weisman^{1,3} has been referred to in those publications. Below, we present for the first time, full details in the syntheses of **Me₂B13N4** and **Me₂Bcyclen**.

2a,7a-Dimethyl-*cis*-decahydro-2a,7a-diaza-4a,9a-diazonia-cyclopenta[cd]phenalene diiodide (2). To a solution of *cis*-decahydro-5*H*-2a,4a,7a,9a-tetraazacyclopenta[cd]phenalene (**1**), prepared according to a literature method,¹⁵ (1.822 g, 8.75 mmol) in acetonitrile (50 mL), iodomethane (9.2 mL, 148 mmol) was added and the flask was then sealed with a septum and the reaction mixture was stirred at room temperature for seven days. The course white solid product precipitated and was collected on a glass frit and was washed with acetonitrile (2 × 10 mL) and diethyl ether (2 × 10 mL) prior to drying under vacuum overnight. Yield = 3.023 g (70%). Electrospray mass spectrometry gave peaks at *m/z* = 365 corresponding to (M – I)⁺ and *m/z* = 119 corresponding to (M – 2I)²⁺. Anal. Calc. for C₁₃H₂₆N₄I₂: C 31.72, H 5.33, N 11.38; found: C 31.77, H 5.26, N 11.25. ¹H NMR (300 MHz, D₂O) δ 1.96 (d, 1H), 2.50–2.29 (m, 1H), 2.76 (td, 1H), 3.39–3.06 (m, 6H), 3.40 (s, 3H, –CH₃), 3.47 (s, 3H, –CH₃), 3.79–3.49 (m, 4H), 3.95–3.83 (m, 2H), 4.16–3.98 (m, 2H), 4.44 (td, 1H), 4.68 (d, 1H), 4.73 (d, 1H). ¹³C{¹H} NMR (75.6 MHz, D₂O) δ 19.0, 42.3, 45.9, 46.2, 46.9, 48.6, 50.5, 51.6, 56.5, 64.2, 65.1, 76.6, 78.2.

4,11-Dimethyl-1,4,8,11-tetraazabicyclo[6.5.2]pentadecane (Me₂B13N4). (3.023 g, 6.14 mmol) of **2** was added to a 500 mL single neck round bottom flask and suspended in 95% ethanol (260 mL). The flask was purged with nitrogen for 15 minutes. While stirring, sodium borohydride (6.97 g, 184 mmol) was added over 5 minutes. The frothy white solution was allowed to stir under nitrogen for 7 days. The excess borohydride was quenched with hydrochloric acid (6 M, 80 mL) and additional HCl was added until the solution reached a pH of two. The ethanol was then removed from the clear solution *in vacuo*. The remaining aqueous solution was made basic with potassium hydroxide (20 mL, 30% w/w) until it reached pH 14 at which point an additional portion of potassium hydroxide was added (5 g). This solution was then extracted with benzene (5 × 150 mL). The benzene extracts were collected and dried over sodium sulfate. After gravity filtration, the excess benzene was removed *in vacuo*. Vacuum distillation from KOH gave a clear oil product. Yield = 1.444 g (98%). Electrospray mass spectrometry gave a single peak at *m/z* = 241 corresponding to (MH)⁺. ¹H NMR (300 MHz, CDCl₃) δ 1.44 (p, 2H, β-CH₂), 2.00 (dt, 1H), 2.13 (s, 3H, –CH₃), 2.31 (s, 3H, –CH₃), 2.36–2.80 (m, 14H), 2.88–2.96 (m, 2H), 3.03–3.21 (m, 2H), 3.22–3.35 (m, 1H). ¹³C{¹H} NMR (75.6 MHz, CDCl₃) δ 25.6, 42.4, 42.9, 51.4, 51.8, 52.9, 53.7, 54.7, 54.8, 55.2, 56.3, 58.0, 59.1. As previously published,³⁶ the free ligand can be

made into the analytically pure hydrochloride salt (**Me₂B13N4**·3HCl·H₂O) by reaction with concentrated HCl in ethanol to produce a white solid which can be recrystallized from methanol–ether. Anal. Calc. for C₁₃H₃₃N₄Cl₃O: C 42.45, H 9.04, N 15.23; found: C 42.39, H 9.19, N 14.88.³⁶

3a,8a-Dimethyl-*cis*-decahydro-5a,10a-diaza-3a,8a-diazonia-pyrene diiodide (4). To a solution of *cis*-decahydro-2a,4a,6a,8a-tetraazacyclopent[fg]acenaphthylene (3), prepared according to a literature method,³⁹ (9.00 g, 46.0 mmol) in acetonitrile (300 mL), iodomethane (43.0 mL, 690 mmol) was added and the flask was then sealed with a septum and the reaction mixture was stirred at room temperature for three days. The white solid product precipitated and was collected on a glass frit and was washed with acetonitrile (2 × 20 mL) and diethyl ether (2 × 20 mL) prior to drying under vacuum overnight. Yield = 20.76 g (94%). Electrospray mass spectrometry gave peaks at *m/z* = 351 corresponding to (M – I)⁺ and *m/z* = 112 corresponding to (M – 2I)²⁺. Anal. Calc. for C₁₂H₂₄N₄I₂: C 30.14, H 5.06, N 11.72; found: C 30.50, H 5.00, N 11.86. ¹H NMR (300 MHz, D₂O) δ 2.98–3.22 (m, 4H), 3.31 (s, 6H, –CH₃), 3.32–3.33 (m, 2H), 3.51–3.61 (m, 4H), 3.37–3.86 (m, 2H) 3.90–4.02 (m, 4H), 4.42 (s, 2H). ¹³C{¹H} NMR (75.6 MHz, D₂O) δ 43.1, 46.6, 46.9, 59.2, 65.0, 78.0.

4,10-Dimethyl-1,4,7,10-tetraazabicyclo[5.5.2]tetraadecane (Me₂Bcyclen). (10.00 g, 21.0 mmol) of **4** was added to a 2-L single neck round bottom flask and suspended in 95% ethanol (800 mL). The flask was purged with nitrogen for 15 minutes. While stirring, sodium borohydride (23.80 g, 630 mmol) was added over 5 minutes. The frothy white solution was allowed to stir under nitrogen for 5 days. The excess borohydride was quenched with 6 M hydrochloric acid, then additional HCl was added until the solution reached a pH of two. The ethanol was then removed from the clear solution *in vacuo*. The remaining aqueous solution was made basic with potassium hydroxide (150 mL, 30% w/w) until it reached pH 14 at which point an additional portion of potassium hydroxide was added (15 g). This solution was then extracted with benzene (5 × 150 mL). The benzene extracts were collected and dried over sodium sulfate. After gravity filtration, the excess benzene was removed *in vacuo*. Vacuum distillation from KOH gave a clear oil product. Yield = 4.51 g (95%). Electrospray mass spectrometry gave a single peak at *m/z* = 227 corresponding to (MH)⁺. ¹H NMR (300 MHz, C₆D₆) δ 2.37 (s, 6H, –CH₃), 2.48–2.55 (m, 4H), 2.75–2.94 (m, 12H), 3.10 (s, 4H). ¹³C{¹H} NMR (75.6 MHz, C₆D₆) δ 44.6, 57.1, 57.5, 60.8. As previously published,³⁶ the free ligand can be made into the analytically pure hydrochloride salt (**Me₂Bcyclen**·3HCl·2H₂O) by reaction with concentrated HCl in ethanol to produce a white solid which can be recrystallized from methanol–ether. Anal. Calc. for C₁₂H₃₃N₄Cl₃O₂: C 38.77, H 8.60, N 15.07; found: C 39.13, H 8.76, N 15.04.³⁶

Metal complexation

Mn(Me₂B13N4)Cl₂. In an inert atmosphere glovebox, 0.240 g (1.0 mmol) of **Me₂B13N4** and 0.126 g (1.0 mmol) of anhydrous MnCl₂ were added to 10 mL of anhydrous aceto-

nitrile in a 4-dram vial. The reaction mixture was stirred at room temperature for 4 days, during which the MnCl₂ and ligand dissolved to give a clear solution. The solution was filtered to remove trace solids, which were discarded, and the solvent evaporated to give a white solid. Yield = 0.329 g (90%). Electrospray mass spectrometry gave a large peak at *m/z* = 330 corresponding to (MnLCl)⁺. Solid state magnetic moment 298 K: μ = 5.95 μ_B. Electronic spectrum, acetonitrile, λ_{max} (nm) [ε (M^{−1} cm^{−1}): <237 nm (>2000)]. Anal. Calc. for Mn(C₁₃H₂₆N₄)Cl₂: C 42.63, H 7.71, N 15.30; found: C 42.30, H 7.92, N 15.37. X-ray quality crystals were grown from ether diffusion into an acetonitrile solution.

Fe(Me₂B13N4)Cl₂. The same procedure as for Mn-(**Me₂B13N4**)Cl₂ was followed, except 0.127 g (1.0 mmol) of anhydrous FeCl₂ was used. The product was a tan solid. Yield = 0.335 g (91%). Electrospray mass spectrometry gave a large peak at *m/z* = 332 corresponding to (FeLCl)⁺. Solid state magnetic moment 298 K: μ = 5.20 μ_B. Electronic spectrum, acetonitrile, λ_{max} (nm) [ε (M^{−1} cm^{−1}): <237 [>2000]; 342 [623]]. Anal. Calc. for Fe(C₁₃H₂₆N₄)Cl₂: C 42.53, H 7.69, N 15.26; found: C 42.42, H 7.85, N 15.07.

[Mn(Me₂B13N4)Cl₂]PF₆. In an inert atmosphere glovebox, the corresponding divalent complex (0.183 g, 0.50 mmol) was dissolved in methanol (10 mL) and ammonium hexafluorophosphate (5 eq., 0.408 g, 2.50 mmol) was added and dissolved. This slightly tan solution was then removed from the glove box and a flow of nitrogen was immediately placed over the surface of the solution. Bromine (2–3 drops) was added and reaction was allowed to stir. (CAUTION! Bromine is toxic. Use only in a chemical fume hood with proper ventilation.) An immediate color change from pale tan to blood red occurred and red precipitate product formed. After 15 minutes, nitrogen was bubbled through the deep red/brown solutions to remove excess bromine. After the excess bromine had been removed (~30 minutes), the solution was placed in a freezer for 30 minutes to finish precipitating the product. The blood red solid product was collected on a glass frit and washed with cold methanol (10 mL) and diethyl ether (2 × 10 mL). Yield = 0.170 g (67%). Electron impact mass spectrometry gave peaks at *m/z* = 365 corresponding to (MnLCl₂)⁺ and *m/z* = 330 corresponding to (MnLCl)⁺. Solid state magnetic moment 298 K: μ = 4.91 μ_B. Electronic spectrum, acetonitrile, λ_{max} (nm) [ε (M^{−1} cm^{−1}): 214 [12 100]; 295 [8600]; 400sh [960]; 526 [512]]. Anal. Calc. for [Mn(C₁₃H₂₈N₄)Cl₂]PF₆: C 30.54, H 5.52, N 10.96; found: C 30.31, H 5.36, N 10.72. X-ray quality crystals were grown from acetone diffusion into a water solution.

[Fe(Me₂B13N4)Cl₂]PF₆. The same procedure as for [Mn-(**Me₂B13N4**)Cl₂]PF₆ was followed, except that 0.184 g, (0.50 mmol) of the divalent iron complex was used. A bright orange/yellow solid product was obtained. Yield = 0.201 g (79%). Electron impact mass spectrometry gave peaks at *m/z* = 366 corresponding to (FeLCl₂)⁺ and *m/z* = 331 corresponding to (FeLCl)⁺. Solid state magnetic moment 298 K: μ = 5.93 μ_B. Electronic spectrum, acetonitrile, λ_{max} (nm) [ε (M^{−1} cm^{−1}): 215 [7000]; 254 [7400]; 358 [3350]]. Anal. Calc. for [Fe(C₁₃H₂₈N₄)Cl₂]PF₆: C 30.49, H 5.51, N 10.49; found: C 30.73, H 5.73, N 10.59.

[Zn(Me₂B13N4)(OAc)(H₂O)]PF₆. In an inert atmosphere glovebox, 0.165 g (0.90 mmol) of anhydrous zinc(II) acetate was suspended in 20 ml anhydrous acetonitrile in a 50 ml round bottom flask. 0.216 g (0.90 mmol) of Me₂B13N4 was separately dissolved in 10 ml of anhydrous acetonitrile and added by pipet to the stirring metal salt suspension. The reaction mixture was stirred at room temperature under nitrogen for 1 day. The clear solution was then removed from the glovebox and evaporated to a colorless oil, which was the crude acetate complex. The oil was dissolved in 3 ml of methanol. A solution of 5 equivalents (4.50 mmol, 0.734 g) of NH₄PF₆ in 5 ml of methanol was added to the stirring complex, which immediately precipitated a white solid. After stirring for 5 minutes, the suspension was stored at −5 °C overnight to complete precipitation of the product. The product was filtered on a glass frit, washed with cold methanol followed by diethyl ether, then dried under vacuum. Yield = 0.211 g (46%). Electrospray mass spectrometry gave a single peak at *m/z* = 363 corresponding to ZnL(OAc)⁺. Anal. Calc. for [Zn(C₁₃H₂₈N₄(C₂H₃O₂)(H₂O)]PF₆: C 34.13, H 6.30, N 10.62; found: C 34.46, H 6.10, N 10.87. X-ray quality crystals were grown by slow evaporation of a water solution.

[Zn(Me₂B13N4)Cl₂]. This complex was synthesized as previously described and analyzed as formulated.³⁷ X-ray quality crystals were grown from ether diffusion into an acetonitrile solution and were formulated as [Zn(Me₂B13N4)Cl(H₂O)]₂[ZnCl₄]·CH₃CN, which may reflect either an impurity or a decomposition product.

[Co(Me₂B13N4)Cl₂]PF₆. This complex was synthesized as previously described and analyzed as formulated.³⁵ X-ray quality crystals of two types were grown from ether diffusion into an acetonitrile solution. Green needles, formulated as [Co(Me₂B13N4)Cl₂]PF₆·CH₃CN, and green plates, formulated as [Co(Me₂B13N4)Cl₂]PF₆, were isolated and solved from the same crystallization sample.

[Cu(Me₂B13N4)Cl]Cl. This complex was synthesized as previously described and analyzed as formulated.³⁷ X-ray quality crystals were grown from ether diffusion into a nitromethane solution.

Crystal structure analysis

Single crystal X-ray diffraction data were collected in series of ω -scans using a Stoe IPSD2 image plate diffractometer utilizing monochromated Mo radiation (λ = 0.71073 Å). Standard procedures were employed for the integration and processing of the data using X-RED.⁵³ Samples were coated in a thin film of perfluoropolyether oil and mounted at the tip of a glass fibre located on a goniometer. Data were collected from crystals held at 150 K in an Oxford Cryosystems nitrogen gas cryostream.

Crystal structures were solved using routine automatic direct methods implemented within SHELXS-97.⁵⁴ Completion of structures was achieved by performing least squares refinement against all unique *F*² values using SHELXL-97.⁵⁴ All non-H atoms were refined with anisotropic displacement parameters. Hydrogen atoms were placed using a riding model.

Where the location of hydrogen atoms was obvious from difference Fourier maps, C–H bond lengths were refined subject to chemically sensible restraints.

Acid decomplexation studies

The designated complexes were used at 1 mM. The complexes' lone d–d absorption was recorded on a Shimadzu UV-3600 UV-Vis-NIR Spectrophotometer in 1 M or 5 M HCl at 90 °C, 50 °C, or 30 °C over time. Typically, isosbestic spectra indicated only one decomposition product as the absorbance at λ_{max} decreased over time. Pseudo first-order conditions allowed the calculation of half-lives from the slopes of the linear ln(absorbance) vs. time plots.

Catalytic sulfide oxidation by complexes

In 5 mL of dry acetonitrile containing 0.1 M thioanisole and 0.33 mM complex, 0.2 mL of 30% H₂O₂ was added to initialize the reaction. The reaction mixture was stirred in a water bath at 303 K for 6 h, and the product analysis was performed by GC using the internal standard method. A parallel experiment without catalyst was conducted as control.

Catalytic hydrogen abstraction by complexes

In 3 mL of methanol–water (1 : 1, v/v) containing 0.05 M 1,4-cyclohexadiene and 1 mM complex, 0.02 mL of 30% H₂O₂ were added to initialize the reaction. The resulting reaction mixture was stirred in a water bath at 303 K for 4 h, and product analysis was conducted by GC using the internal standard method. A parallel experiment without catalyst was conducted as control.

Acknowledgements

TJH acknowledges Southwestern Oklahoma State University for internal funding through a Proposal Development Award. TJH acknowledges the Donors of the American Chemical Society Petroleum Research Fund; Health Research award for project number HR13-157, from the Oklahoma Center for the Advancement of Science and Technology; and Grant Number P20RR016478 from the National Center for Research Resources (NCRR), a component of the National Institutes of Health (NIH) for partial support of this research. TJH also acknowledges the Henry Dreyfus Teacher-Scholar Awards Program for support of this work. GY acknowledges support from the National Natural Science Foundation of China (NSFC no. 21273086).

Notes and references

- 1 G. R. Weisman, M. E. Rogers, E. H. Wong, J. P. Jasinski and E. S. Paight, *J. Am. Chem. Soc.*, 1990, **112**, 8604–8605.
- 2 A. Bencini, A. Bianchi, C. Bazzicalupi, M. Ciampolini, V. Fusi, M. Micheloni, N. Nardi, P. Paoli and B. Valtancoli, *Supramol. Chem.*, 1994, **3**, 141–146.

- 3 G. R. Weisman, E. H. Wong, D. C. Hill, M. E. Rogers, D. P. Reed and J. C. Calabrese, *Chem. Commun.*, 1996, 947–948.
- 4 E. H. Wong, G. R. Weisman, D. C. Hill, D. P. Reed, M. E. Rogers, J. P. Condon, M. A. Fagan, J. C. Calabrese, K.-C. Lam, I. A. Guzei and A. L. Rheingold, *J. Am. Chem. Soc.*, 2000, **122**, 10561–10572.
- 5 X. Sun, M. Wuest, G. R. Weisman, E. H. Wong, D. P. Reed, C. A. Boswell, R. Motekaitis, A. E. Martell, M. J. Welch and C. J. Anderson, *J. Med. Chem.*, 2002, **45**, 469–477.
- 6 J. E. Sprague, Y. Peng, X. Sun, G. R. Weisman, E. H. Wong, S. Achilefu and C. J. Anderson, *Clin. Cancer Res.*, 2004, **10**, 8674–8682.
- 7 W. Niu, E. H. Wong, G. R. Weisman, L. N. Zakharov, C. D. Incarvito and A. L. Rheingold, *Polyhedron*, 2004, **23**, 1019–1025.
- 8 C. A. Boswell, X. Sun, W. Niu, G. R. Weisman, E. H. Wong, A. L. Rheingold and C. J. Anderson, *J. Med. Chem.*, 2004, **47**, 1465–1474.
- 9 K. S. Woodin, K. J. Heroux, C. A. Boswell, E. H. Wong, G. R. Weisman, W. Niu, S. A. Tomellini, C. J. Anderson, L. N. Zakharov and A. L. Rheingold, *Eur. J. Inorg. Chem.*, 2005, **7**, 4829–4833.
- 10 C. A. Boswell, P. McQuade, G. R. Weisman, E. H. Wong and C. J. Anderson, *Nucl. Med. Biol.*, 2005, **32**, 29–38.
- 11 K. J. Heroux, K. S. Woodin, D. J. Tranchemontagne, P. C. B. Widger, E. Southwick, E. H. Wong, G. R. Weisman, S. A. Tomellini, T. J. Wadas, C. J. Anderson, S. Kassel, J. A. Golen and A. L. Rheingold, *Dalton Trans.*, 2007, 2150–2162.
- 12 J. E. Sprague, Y. Peng, A. L. Fiamengo, K. S. Woodin, E. A. Southwick, G. R. Wiesman, E. H. Wong, J. A. Golen, A. L. Rheingold and C. J. Anderson, *J. Med. Chem.*, 2007, **50**, 2527–2535.
- 13 C. J. Anderson, T. J. Wadas, E. H. Wong and G. R. Weisman, *Q. J. Nuc. Med. Mol. Imaging*, 2008, **52**, 185–192.
- 14 D. J. Stigers, R. Ferdani, G. R. Weisman, E. H. Wong, C. J. Anderson, J. A. Golen, C. Moore and A. L. Rheingold, *Dalton Trans.*, 2010, **39**, 1699–1701.
- 15 A. Y. Odendaal, A. L. Fiamengo, R. Ferdani, T. J. Wadas, D. C. Hill, Y. Peng, K. J. Heroux, J. A. Golen, A. L. Rheingold, C. J. Anderson, G. R. Weisman and E. H. Wong, *Inorg. Chem.*, 2011, **50**, 3078–3086.
- 16 P. Desogere, C. Bernhard, C. Goze, M.-J. Penouilh, Y. Rousselin and F. Denat, *Eur. J. Org. Chem.*, 2013, 1538–1545.
- 17 T. J. Hubin, J. M. McCormick, S. R. Collinson, N. W. Alcock and D. H. Busch, *Chem. Commun.*, 1998, 1675–1676.
- 18 T. J. Hubin, J. M. McCormick, S. R. Collinson, M. Buchalova, C. M. Perkins, N. W. Alcock, P. K. Kahol, A. Raghunathan and D. H. Busch, *J. Am. Chem. Soc.*, 2000, **122**, 2512–2522.
- 19 T. J. Hubin, J. M. McCormick, N. W. Alcock and D. H. Busch, *Inorg. Chem.*, 2001, **40**, 435–444.
- 20 T. J. Hubin, J. M. McCormick, S. R. Collinson, N. W. Alcock, H. J. Clase and D. H. Busch, *Inorg. Chim. Acta*, 2003, **346**, 76–86.
- 21 G. Yin, M. Buchalova, A. M. Danby, C. M. Perkins, D. Kitko, J. D. Carter, W. M. Scheper and D. H. Busch, *J. Am. Chem. Soc.*, 2005, **127**, 17170–17171.
- 22 G. Yin, J. M. McCormick, M. Buchalova, A. M. Danby, K. Rodgers, V. W. Day, K. Smith, C. M. Perkins, D. Kitko, J. D. Carter, W. M. Scheper and D. H. Busch, *Inorg. Chem.*, 2006, **45**, 8052–8061.
- 23 G. Yin, A. M. Danby, D. Kitko, J. D. Carter, W. M. Scheper and D. H. Busch, *J. Am. Chem. Soc.*, 2007, **129**, 1512–1513.
- 24 G. Yin, A. M. Danby, D. Kitko, J. D. Carter, W. M. Scheper and D. H. Busch, *Inorg. Chem.*, 2007, **46**, 2173–2180.
- 25 G. Yin, A. M. Danby, D. Kitko, J. D. Carter, W. M. Scheper and D. H. Busch, *J. Am. Chem. Soc.*, 2008, **130**, 16245–16253.
- 26 S. Shi, Y. Wang, A. Xu, H. Wang, D. Zhu, S. B. Roy, T. A. Jackson, D. H. Busch and G. Yin, *Angew. Chem., Int. Ed.*, 2011, **50**, 7321–7324.
- 27 Y. Wang, S. Shi, D. Zhu and G. Yin, *Dalton Trans.*, 2012, **41**, 2612–2619.
- 28 Y. Wang, S. Shi, H. Wang, D. Zhu and G. Yin, *Chem. Commun.*, 2012, **48**, 7832–7834.
- 29 Y. Wang, J. Sheng, S. Shi, D. Zhu and G. Yin, *J. Phys. Chem. C*, 2012, **116**, 13231–13239.
- 30 L. Dong, Y. Wang, Y. Lu, Z. Chen, F. Mei, H. Xiong and G. Yin, *Inorg. Chem.*, 2013, **52**, 5418–5427.
- 31 T. J. Hubin, *Coord. Chem. Rev.*, 2003, **241**, 27–46.
- 32 G. Yin, *Acc. Chem. Res.*, 2013, **46**, 483–492.
- 33 D. H. Busch, S. R. Collinson and T. J. Hubin, *Catalysts and methods for catalytic oxidation*, US Patent 6,906,189, 14 June 2005.
- 34 Z. Zhang, K. L. Coats, Z. Chen, T. J. Hubin and G. Yin, *Inorg. Chem.*, 2014, **53**, 11937–11947.
- 35 T. J. Hubin, N. W. Alcock, H. J. Clase, L. L. Seib and D. H. Busch, *Inorg. Chim. Acta*, 2002, **337**, 91–102.
- 36 T. J. Hubin, N. W. Alcock, H. J. Clase and D. H. Busch, *Supramol. Chem.*, 2001, **13**, 261–276.
- 37 T. J. Hubin, N. W. Alcock, M. D. Morton and D. H. Busch, *Inorg. Chim. Acta*, 2003, **348**, 33–40.
- 38 W. Niu, E. H. Wong, G. R. Weisman, K.-C. Lam and A. L. Rheingold, *Inorg. Chem. Commun.*, 1999, **2**, 361–363.
- 39 M. Le Baccon, F. Chuburu, L. Toupet, H. Handel, M. Soibinet, I. Deschamps-Olivier, J.-P. Barbier and M. Aplincourt, *New J. Chem.*, 2001, **25**, 1168–1174.
- 40 J. Rohovec, R. Gyepes, I. Cisarova, J. Rudovsky and I. Lukes, Nucleophilic reactivity of perhydro-3,6,9,12-tetraazacyclopenteno[1,3-f,g]acenaphthylene. A unified approach to N-monosubstituted and N,N'-disubstituted cyclen derivatives, *Tetrahedron Lett.*, 2000, **41**, 1249–1253.
- 41 T. J. Hubin, J. M. McCormick, N. W. Alcock, H. J. Clase and D. H. Busch, *Inorg. Chem.*, 1999, **38**, 4435–4446.
- 42 T. J. Hubin, J. M. McCormick, N. W. Alcock and D. H. Busch, *Inorg. Chem.*, 2001, **40**, 435–444.

- 43 J. M. McClain II, D. L. Maples, R. D. Maples, D. L. Matz, S. M. Harris, A. D. L. Nelson, J. D. Silversides, S. J. Archibald and T. J. Hubin, *Acta Crystallogr., Sect. C: Cryst. Struct. Commun.*, 2006, **62**, m553–m555.
- 44 D. L. Maples, R. D. Maples, W. A. Hoffert, T. H. Parsell, A. van Asselt, J. D. Silversides, S. J. Archibald and T. J. Hubin, *Inorg. Chim. Acta*, 2009, **362**, 2084–2088.
- 45 T. J. Prior, D. L. Maples, R. D. Maples, W. A. Hoffert, T. H. Parsell, J. D. Silversides, S. J. Archibald and T. J. Hubin, *Acta Crystallogr., Sect. E: Struct. Rep. Online*, 2014, **70**, 148–152.
- 46 A. Y. Odendaal, Ph.D. Thesis, University of New Hampshire, Durham, N.H., 2009.
- 47 D. G. Jones, K. R. Wilson, D. J. Cannon-Smith, A. D. Shircliff, Z. Zhang, Z. Chen, T. J. Prior, G. Yin and T. J. Hubin, *Inorg. Chem.*, 2015, **54**, 2221–2234.
- 48 K. Burger, *Coordination Chemistry: Experimental Methods*, Butterworth, London, 1973.
- 49 A. B. P. Lever, *Inorganic Electronic Spectroscopy*, Elsevier, Amsterdam, 2nd edn, 1984.
- 50 Y. Feng, J. England and L. J. Que, *ACS Catal.*, 2011, **1**, 1035–1042.
- 51 C. T. Goldsmith and T. D. P. Stack, *Inorg. Chem.*, 2006, **45**, 6048–6055.
- 52 C. M. McGinley and W. A. van der Donk, *Chem. Commun.*, 2003, 2843–2846.
- 53 *X-AREA v 1.64*, STOE & Cie GmbH, Darmstadt, 2012.
- 54 G. Sheldrick, *Acta Crystallogr., Sect. A: Fundam Crystallogr.*, 2008, **64**, 112–122.